

# Instability of Hydrocarbon Films over Mineral Surfaces: Microscale Experimental Studies

Franco M. Francisca<sup>1</sup>; Victor A. Rinaldi<sup>2</sup>; and Juan C. Santamarina<sup>3</sup>

**Abstract:** The fluid-mineral interaction defines the affinity of mineral surfaces for water in the presence of oil, determines wettability, affects interparticle forces, and controls the effectiveness of soil decontamination and oil recovery from reservoirs. This study involves the use of electrical impedance measurements and optical microscopy to determine the rupture time of thin oil films on mineral surfaces when water droplets are placed on the film. The results show that the time for film rupture depends on the mineral and the type of oil, it increases with the increase in oil viscosity, and it decreases in the presence of surfactants. The instability and rupture of the thin hydrocarbon films are analyzed taking into consideration surface forces and disjoining/conjoining pressure. These results are relevant to defining the ability of mineral surfaces to become wetted by water, leading to the displacement of organic films.

**DOI:** 10.1061/(ASCE)0733-9372(2003)129:12(1120)

**CE Database subject headings:** Biofilm; Oil recovery; Porous media; Hydrocarbons; Mineral deposits.

## Introduction

The displacement of organic fluids in porous media affects oil recovery from porous rocks and decontamination efforts in the near surface; viscous, interfacial, and gravity forces are involved (Arman 1992; Dullien 1992; Abriola et al. 1993; Udell et al. 1995; Martel et al. 1998). Most experimental studies are conducted at the macroscale and are designed to determine optimal conditions for oil recovery and decontamination (Zettlemoyer 1969; Anderson 1986; Morrow 1990; Pennell et al. 1993; Lunn and Kueper 1999). Such experimental results confirm the difficulty in extracting the organic fluid from the medium, particularly when the mineral surfaces have adsorbed a water-repellent agent, i.e., multiphase fluid flow depends on the wettability of the mineral surfaces. Therefore, the macroscale response is controlled by microscale physical-chemical phenomena that take place at the interface between the fluids and the surface.

However, only a few studies have been conducted at the microscale. Robin et al. (1995) used cryo-scanning electron microscopy to monitor oil displacement inside porous media and related the surface wettability to the mineralogy. Basu and Sharma (1996) used atomic force microscopy and showed the effect of fluid pH, salinity, and surface roughness on the forces of interaction between hydrocarbons and mineral surfaces. Sharma and Re-

iter (1996) studied the influence of force interactions on film rupture, and drop formation. Basu et al. (1998) observed oil displacement by water in sand, and showed that the oil drop that formed was asymmetric, probably due to surface heterogeneity and roughness.

The microscale study presented herein centers on the disjoining of the organic phase from the mineral surface, with emphasis on the time required for the rupture of adsorbed organic films, and the relation between rupture and the affinity between the mineral and the fluids.

## Underlying Physical Concepts

A brief review of fundamental physical processes and phenomena is presented in this section, including interfacial tension, contact angle, capillarity, and thin films.

### Interfacial Tension

When a liquid is in contact with a gas, another immiscible fluid, or a solid, intermolecular attraction within the liquid is unbalanced at the interface, resulting in interfacial tension  $\sigma$ , i.e., the tendency for the surface to shrink. In terms of energy, the interfacial tension  $\sigma$  for two immiscible fluids in contact is (Defay and Prigogine 1966)

$$\sigma = G - \sum_i \Gamma_i \mu_i \quad (1)$$

where  $G$ =Gibbs free energy per unit area;  $\Gamma_i$ =adsorption of the element  $i$  in moles ( $n$ ) per unit area; and  $\mu_i$ =chemical potential of the element (i.e., the energy contribution for the addition of  $n$  moles of the element). Therefore, the interfacial tension  $\sigma$  is equal to the free surface energy per unit area,  $G$ , if the system is in physical-chemical equilibrium, that is,  $\sum_i \Gamma_i \mu_i = 0$ . For an ideal two-phase system, in which the phases are homogeneous and the thickness of the interface is practically null, the Gibbs free energy per unit area  $G$  is (Defay and Prigogine 1966; Lyklema 1991)

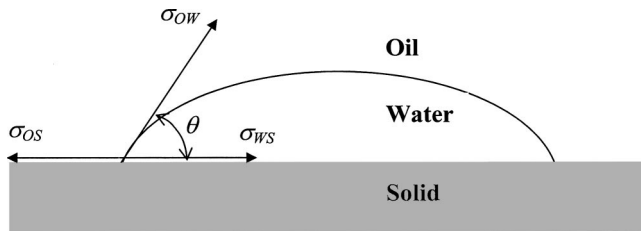
$$G = u - Ts \quad (2)$$

<sup>1</sup>Assistant Professor, Civil Engineering Dept., National Univ. of Córdoba, Postdoctoral Fellow CONICET, Cordoba, Velez Sarsfield 1601, 5000, Argentina.

<sup>2</sup>Associate Professor, Civil Engineering Dept., National Univ. of Córdoba, Researcher CONICET, Cordoba, Velez Sarsfield 1601, 5000, Argentina.

<sup>3</sup>Professor, School of Civil and Environmental Engineering, Georgia Institute of Technology, Atlanta, GA 30332.

Note. Associate Editor: Robert G. Arnold. Discussion open until May 1, 2004. Separate discussions must be submitted for individual papers. To extend the closing date by one month, a written request must be filed with the ASCE Managing Editor. The manuscript for this paper was submitted for review and possible publication on January 9, 2001; approved on September 23, 2002. This paper is part of the *Journal of Environmental Engineering*, Vol. 129, No. 12, December 1, 2003. ©ASCE, ISSN 0733-9372/2003/12-1120-1128/\$18.00.



Wettability	Contact Angle $\theta$	Schematic Representation
Water-wet	$0^\circ$ to $\sim 70^\circ$	
Neutrally wet	$\sim 70^\circ$ to $\sim 110^\circ$	
Oil-wet	$\sim 110^\circ$ to $180^\circ$	

**Fig. 1.** Wettability of solid surfaces defined by the contact angle. Usual ranges for water-wet, neutrally wet, or oil-wet surfaces. (Note that water-wet or oil-wet conditions are established by testing the substrate with the two fluids present at the same time.)

where  $T$ =absolute temperature;  $u$ =system energy per unit area; and  $s$ =entropy normalized by area.

Interfacial tension controls the wetting of mineral surfaces and the displacement of organic fluids in soils and porous rocks. The use of surfactants and alcohol in soil remediation is designed to alter the interfacial tension (e.g., Abdul et al. 1990).

### Wettability and Contact Angle

The wettability of a mineral is the ability of a fluid to spread over its surface in the presence of another immiscible fluid. It depends on the interfacial tension and the fluid viscosity (Corey 1986). Therefore, when water and a low-viscosity oil are discharged in a porous medium, the oil wets the surface first because of its low interfacial tension in contact with air. Afterward, the water may displace the oil. The remainder of this paper emphasizes the role of interfacial tension.

Different methods are used to define the wettability of a system. Quantitative methods include contact angle measurements, the imbibition and displacement test (Amott's test), and measurement of pressure-saturation curves in the centrifuge (Dullien 1992). Indirect or qualitative methods include relative permeability, microscopic examination, flotation, imbibition rates, displacement capillary pressure, and nuclear magnetic resonance. These techniques are discussed by Anderson (1986).

When two nonmiscible fluids are in contact with a solid, each fluid-fluid and fluid-solid interface tries to shrink because of interfacial tension. As a result, the interface between the two fluids is at a "contact angle"  $\theta$  with the solid substrate. From equilibrium considerations, the sum of forces parallel to the solid surface gives [Fig. 1; details in Adamson and Gast (1997); Young developed the general form of this relation in 1805]

$$\cos \theta = \frac{\sigma_{OS} - \sigma_{WS}}{\sigma_{OW}} \quad (3)$$

where  $\sigma_{OW}$ ,  $\sigma_{OS}$ , and  $\sigma_{WS}$  are the values of interfacial tension between oil and water, oil and solid, and water and solid, respectively. The indices "O" and "W" can represent different nonwetting and wetting phases, respectively. By convention, the contact angle is measured with respect to water.

Mineral surfaces are classified as water wet or oil wet depending on their relative preference to be wetted by either water or oil (Morrow 1990). The assessment of wettability from contact angle measurements is summarized in Fig. 1. The water-wet or oil-wet conditions are established by testing the substrate with the two fluids present at the same time, rather than a single fluid and air. Usually, mineral surfaces in soils and rocks are hydrophilic and the water-wet condition prevails. The oil-wet condition may result when a water-repellent agent (for example, silicone) is absorbed at the surface. Chemisorption of organic matter on the mineral surfaces may also create a hydrophobic surface. However, since mineral surfaces are hydrophilic in nature, the oil-wet condition can be considered a temporary condition. Thus, given enough time, organic fluids tend to be displaced by water.

If the surrounding fluid is air, the surface tensions between vapor and solid  $\sigma_{vs}$ , liquid and solid  $\sigma_{ls}$ , and liquid and vapor  $\sigma_{lv}$  are the main parameters and Eq. (3) is written as  $\cos \theta = (\sigma_{vs} - \sigma_{ls})/\sigma_{lv}$ . It follows from Eqs. (1), (2), and (3) that the effects of temperature, pressure, chemical composition, and pH on the wetting of solid surfaces can be investigated by mean of contact angle measurements.

Various techniques are used to determine the contact angle, including the tilting plate method, sessile drop, and sessile bubble (see, for example, Shaw 1977; Dullien 1992). The apparent simplicity in the determination of contact angle is misleading, from the point of view of both measurement and interpretation (a comprehensive review can be found in Kwok and Neumann 1999). In particular, there is hysteresis in the contact angle  $\theta$  with respect to the direction of fluid motion. There are two possible causes for contact angle hysteresis (Adamson and Gast 1997; Extrand 1998). First, there is the effect of surface roughness, whereby the macroscopically observed angle differs from the contact angle at the scale of asperities, which is the scale relevant to Young's equation. Second, the contact angle is affected by surface heterogeneity due to the alteration of surface properties by fluids and the presence of surfactants or surface-active agents. While emphasis should be placed on the advancing angle, the equilibrium values in advancing  $\theta_a$  and receding  $\theta_r$  motions are often reported. Extrand and Kumagai (1997) propose the dimensionless parameter  $H = (\theta_a - \theta_r)/\theta_a$  to quantify hysteresis and observe that  $H$  is about the same for a given solid surface, regardless of the fluid. In view of these observations, contact angle measurements on soil surfaces and on porous rocks require careful interpretation.

### Capillary Pressure

Consider a capillary tube filled with a wetting fluid from one end and with a nonwetting fluid from the other. The interfacial tension  $\sigma$  between the two fluids and the contact angle  $\theta$  formed by the fluid interface on the tube wall determine the pressure difference that develops in the two fluids. This is the capillary pressure  $P_c$ ; at equilibrium

$$P_c = P_{NW} - P_W = \frac{2\sigma \cos \theta}{r} \quad (4)$$

where  $P_{NW}$  and  $P_W$ =fluid pressures in the nonwetting and wetting phases, respectively; and  $r$ =the radius of the capillary tube. Observe that the smaller the tube or "pore size," the greater the

**Table 1.** Selected Minerals: Physical and Mineralogical Properties

Property	Calcite	Quartz	Biotite	Muscovite
Chemical formula	CaCO <sub>3</sub>	SiO <sub>2</sub>	K(Mg,Fe) <sub>3</sub> (AlSi <sub>3</sub> O <sub>10</sub> )(OH) <sub>2</sub>	KAl <sub>2</sub> (AlSi <sub>3</sub> O <sub>10</sub> )(OH) <sub>2</sub>
Crystallographic system	Hexagonal	Hexagonal	Monoclinic	Monoclinic
Unit cell	<i>a</i> = 4.99 Å <i>c</i> = 17.06 Å	<i>a</i> = 4.91 Å <i>c</i> = 5.41 Å	<i>a</i> = 5.31 Å <i>b</i> = 9.23 Å <i>c</i> = 10.18 Å $\alpha$ = 99° 18'	<i>a</i> = 5.19 Å <i>b</i> = 9.04 Å <i>c</i> = 20.08 Å $\alpha$ = 95° 30'
Miller index	(10–11) perfect	(10–11)	(001) perfect	(001) with presence of (110)
<i>G<sub>s</sub></i> (specific gravity)	2.71	2.65	2.8–3.2	2.76–2.88
Mohr hardness	3	7	2 1/2–3	2–2 1/2
Color	Transparent	Transparent	Green to black	Colorless

Note: Data compiled from Klein and Hurlbut (1999).

pressure required to displace the interface (implications are discussed by Mercer and Cohen 1990; Dullien 1992; Pennell et al. 1996; Mani and Mohanty 1997; Martel et al. 1998; Cho and Santamarina 2001).

### **Thin Films: Molecular-Level Forces, Disjoining Pressure, and Instability**

When a fluid is displaced by another fluid, a film of the original fluid may remain in contact with the mineral surface coating the pore walls or it may eventually rupture. Film rupture is an instability mechanism governed by molecular-level repulsion and attraction forces (these forces are reviewed by Lyklema 1991; Israelachvili 1992; Adamson and Gast 1997).

The organization of molecules in the fluid near the mineral substrate is affected by the mineral structure through geometric effects and by Born, Coulombian, van der Waals, and hydrophobic forces. The Born repulsion force (which gives molecules their “hard shell” appearance), limited molecular mobility, and regular molecular arrangement cause an oscillatory force-distance response within the few monolayers near the mineral surface, i.e., about ten monolayers or less. Ghatak et al. (1999) studied the formation of holes in thin films and took into consideration the contribution of these short-range effects.

If a thin film separates another fluid from the mineral surface, a van der Waals interaction develops between the remote fluid and the mineral. If the thin film is nonpolar, counterions remain on the mineral surface, neutralizing the effective surface charge. When the polar water molecules reach the mineral surface, counterions are hydrated and double layer interaction forces develop (which can be analyzed from electrostatics or osmotic effects). Finally, the hydrophobic force is a long-range attraction force, much stronger than the force produced by van der Waals interactions, and it develops between hydrophobic surfaces in aqueous solutions. Tsekov and Schulze (1997) proposed an expression for considering the hydrophobic forces acting in thin films.

The combined effect of these forces is summarized and quantified as an excess pressure, called the “disjoining/conjoining pressure”  $\Pi$  (Bergeron 1999). The disjoining/conjoining pressure can also be defined as the negative derivative of the free energy per unit area,  $G$ , with respect to the film thickness  $h$

$$\Pi = - \frac{\partial G(h)}{\partial h} \quad (5)$$

The disjoining/conjoining pressure is affected by the curvature of the surface. For zero-curvature solid surfaces, the disjoining/conjoining pressure is equal to the capillary pressure, because  $\Pi$

in mechanical equilibrium is equal to the difference between the normal pressure at the interface and the pressure in the bulk of the phase (Morrow 1990; Sharma and Reiter 1996; Bergeron 1999).

The disjoining/conjoining pressure governs the system stability and the rupture of films: films are unstable when  $\partial\Pi/\partial h > 0$ , i.e., the second derivative of the free energy  $G$  with respect to distance  $h$  is negative (Lyklema 1991; Reiter et al. 1999).

Basu and Sharma (1996) and Basu et al. (1996) studied the effects of pH, salinity, and surface characteristics on wetting and film rupture. In the case of organic films, they observe that thin film stability increases when the pH of the aqueous liquid decreases and when surfaces lack asperities or irregularities.

### **Experimental Procedures and Test Devices**

The purpose of this study was to investigate the wetting behavior of mineral surfaces, with emphasis on film instability. Contact angles were measured first, followed by the evaluation of film rupture.

#### **Contact Angle**

The selected minerals are abundant in prevailing formations, and include calcite, biotite (common in the silt and clay soil particles of desert regions), quartz crystal, and muscovite (common in soils from temperate regions with abundant vegetation). The selected fluids include deionized water, paraffin oil, silicone oil, lubricant oil, and isopropyl alcohol. Tables 1 and 2 summarize the most relevant properties of these minerals and fluids.

Fresh cleavage planes and natural crystal surfaces were tested without polishing to obtain contact angle values representative for these minerals in their natural state. (Note: the scale of roughness in the vicinity of the measurement is much smaller than the scale of the observation in all cases.) Before testing, surfaces were cleaned with a detergent and alcohol solution to remove all possible contamination, and then oven dried at 150°C. After drying, minerals were positioned so that their top face was horizontal. All minerals and fluids were at room temperature during the tests. A drop of fluid was released over the mineral surface with a needle; drop diameters ranged between 4 and 7 mm to avoid size effects that are produced by gravity forces and by surface roughness (Drelich et al. 1996). Finally, contact angles were measured after a stabilization period of approximately 30 min, by focusing the optical microscope at the initial tangent formed by the drop on the horizontal surface (magnification 40×–150×).

**Table 2.** Physical Characteristics of Selected Fluids

Property	Water	Paraffin oil	Silicone oil	Lubricant oil	Isopropyl alcohol
Chemical formula	H <sub>2</sub> O	C <sub>n</sub> H <sub>2n+2</sub>	(CH <sub>3</sub> ) <sub>2</sub> SiCl <sub>2</sub>	Mixture of hydrocarbons	C <sub>3</sub> H <sub>8</sub> O
Unit weight (kN/m <sup>3</sup> )	9.81	6.94	9.63	8.88	7.9
Color	Colorless	Colorless	Yellowish	Yellowish	Colorless
Permittivity <sup>a</sup> κ'	78.5	2.01	2.2–2.8	2.43	34.7
Interfacial tension <sup>b</sup> (N/m)	0.073	0.027	0.035	0.025 <sup>c</sup>	0.022
Odor	Odorless	Odorless	Aromatic	Aromatic	Aromatic
Viscosity <sup>b</sup> (cm <sup>2</sup> /s)	1.0	2.7	1,000.0	112.6	3.3
Viscosity of the crude oil <sup>b</sup> (cm <sup>2</sup> /s)		Low viscosity (LV)			2.6
		Medium viscosity (MV)			24
		High viscosity (HV)			3,000

Note: Sources: this study; manufacturers; CRC Handbook (1988); Irwin et al. (1997).

<sup>a</sup>At 200 MHz.

<sup>b</sup>In air at 20°C.

<sup>c</sup>Computed.

### Film Rupture

Two different procedures were used to study the rupture of thin organic films when water was added. The first technique consisted of an indirect determination of film rupture based on electrical impedance measurements. The second method involved the direct microscope-based observation of film rupture.

### Electrical Impedance Measurements

A NaCl crystal substrate was used for this study so that changes in electrical conductivity would be magnified upon water wetting. Different films were formed using paraffin oil, lubricant oil, and three crude oils of different viscosities (Table 2). Two electrodes 3.5 mm apart were positioned normal to the crystal surface, at a distance of 1 mm from the surface (Fig. 2). A drop of water was placed with a needle over the film, between the electrodes. Approximately 2.5 mm of the electrode length remained inside the water droplet. The electrical impedance was monitored with an impedance analyzer (HP 4192) operating at 0.2 MHz to avoid electrode polarization effects (accuracy of 0.15% for impedance 10 kΩ–10<sup>3</sup> MΩ).

### Optical Microscopy

The time for film rupture after adding the water droplet was also determined by direct optical observation with the aid of a standard optical microscope. Minerals (salt, muscovite, biotite, calcite, and quartz) and man-made materials (glass and plexiglas) were used as substrates. Glass was included since its principal component is amorphous silica, and thus the results can be compared with those obtained for quartz and the effect of the crystal inner structure could be evaluated. Plexiglas was included as a reference material due to its hydrophobic nature (plexiglas is an organic compound, methyl methacrylate, and exhibits affinity for

organic fluids). The substrates were oven dried and then allowed to reach room temperature with the top surface on a horizontal plane. The surfaces were then coated with the three oils of different viscosities (this test required nontransparent film to facilitate visualization). Finally, a drop of the wetting fluid, 5–7 mm in size, was released with the aid of a needle on the film; the selected wetting fluids included deionized water, water-detergent solution, and isopropyl alcohol.

## Experimental Results

### Contact Angle

Table 3 summarizes the measured contact angles. The highest contact angles for all minerals were observed for water. This is in agreement with the high liquid-vapor interfacial tension for water (Table 2). Given the small contact angles measured for the organic fluids, it follows from Young's equation that  $\sigma_{vs} - \sigma_{is} \approx \sigma_{lv}$ .

The contact angles measured with all fluids are highest for calcite (see also Ethington 1990). For a given fluid,  $\sigma_{lv}$  is the same for all minerals. Therefore, the lower contact angle observed in quartz, muscovite, and biotite suggests a decrease  $\sigma_{is}$  relative to  $\sigma_{vs}$  in these minerals, i.e., a higher tendency to be wetted by the fluids (Fig. 1). The crystal structure of minerals explains the different affinity for fluids. For example, when crystallization takes place in an aqueous environment, groups with water affinity develop on the surface, and the contact angle that water forms on the crystal is lower than the angle observed in the same mineral crystallized in air (Shaw 1977). Therefore, the crystalline structure and surface conditions at the atomic scale influence the interaction between phases and the measured contact angles.

**Table 3.** Contact Angle in Air Measured by Drop-in-Equilibrium Technique Aided by Optical Microscopy

Property	Water	Paraffin oil	Silicone oil	Lubricant oil	Isopropyl alcohol
Calcite	49.6±7.9	8.8±1.8	≈0	22.4±2.3	22.9±3.8
Quartz	13.1±2.0	≈0	≈0	7.5±1.4	≈0
Biotite	32.6±2.9	≈0	≈0	7.0±1.5	9.5±1.4
Muscovite	16.6±3.5	≈0	≈0	9.9±2.4	≈0

Contact angle for water on glass is  $\theta=52.7\pm2.9^\circ$  and on plexiglas is  $\theta=65.6\pm4.8^\circ$ .

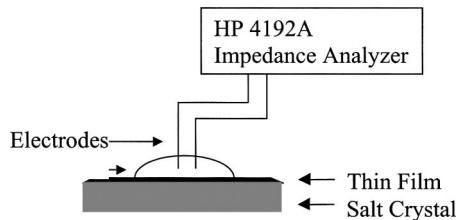


**Fig. 2.** Film rupture monitoring using electrical impedance measurements: Schematic representation of measurement procedure and devices

The effect of surfactants on wettability was studied by determining the contact angle between calcite and water mixed with 10% of commercial detergent. The contact angle for calcite-air-water ( $49.6 \pm 7.9^\circ$ , Table 3) reduces to  $17.0 \pm 2.6^\circ$  when detergent is added. It follows from Eq. (3) that the optimum effect of the surfactant would be to simultaneously reduce both  $\sigma_{ow}$  and  $\sigma_{ws}$ .

### Film Rupture

#### Preliminary Observations

The detailed observation of oil-wet mineral surfaces after drops of water were placed on the film show the following characteristic sequence of events:

1. The thickness of the organic film over the mineral surface gradually decreases at different locations on the surface, and small holes start developing in the film. Surface asperities facilitate the development of holes.

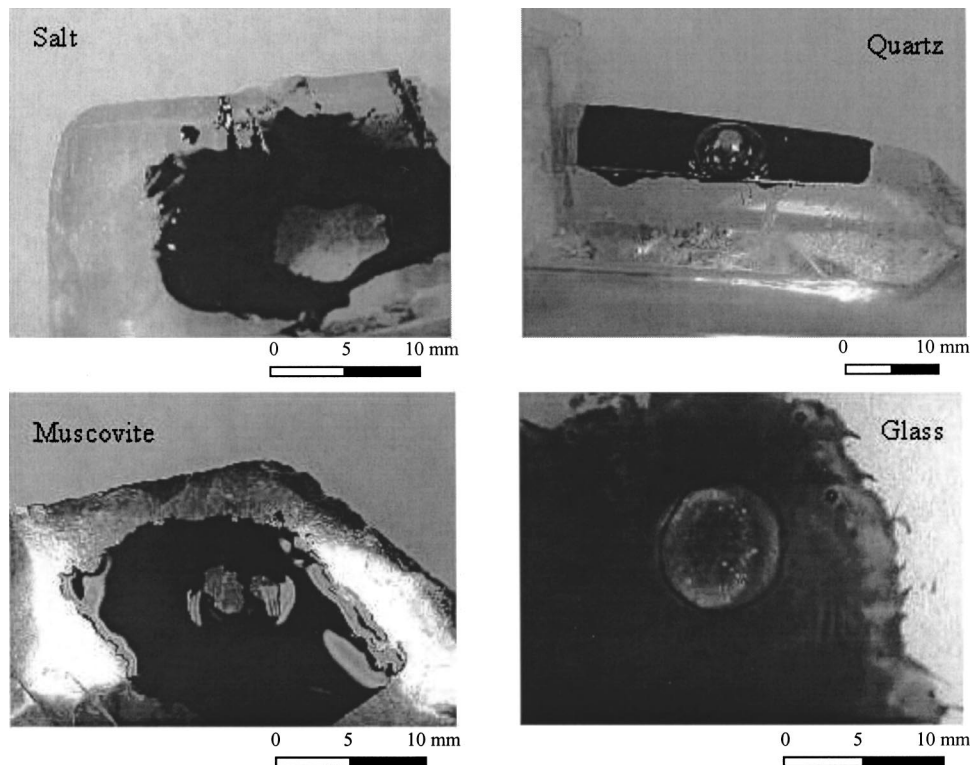
2. The size of holes increases. The film becomes unstable and it ruptures, leaving large openings where water reaches the mineral surface.
3. At these openings, a solid-water-oil interface develops, the contact line recedes, and the oil film is transformed into droplets on the mineral surface. These droplets may eventually detach.

Final measurements were performed on fresh cleavage planes and crystal planes which are optically smooth (optical microscopy). Fig. 3 shows photographs of ruptured petroleum films on salt crystal (a), quartz (b), muscovite (c), and glass (d) after adding a water drop. Sharma and Reiter (1996) make similar observations and conclude that the thicker the film, the smaller the number of initial holes, the greater the final size of holes that appear when the film breaks, and the larger the diameter of the final oil droplets.

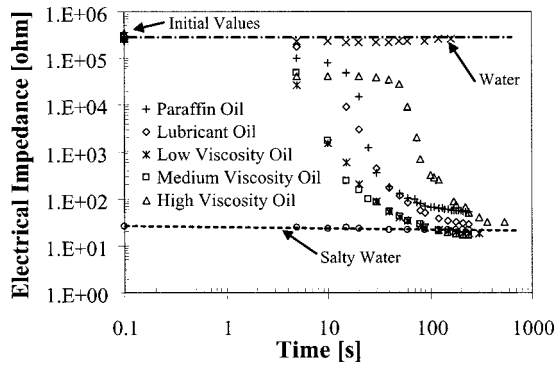
#### Electrical Impedance Measurements

Fig. 4 shows the evolution of electrical impedance with time, for different organic films. The initial impedance of the water was  $\sim 2.6 \times 10^5 \Omega$ . The first break in the impedance trend is observed soon after the water drop is added, and it coincides with the development of small holes in the film (usually within the first 5 s). Soon afterward, the impedance decreases as the salt substrate hydrates forming an electrolyte. Further access to the surface accentuates the hydration process and the impedance eventually decreases by almost four orders of magnitude, reaching  $\sim 20 \Omega$ , which is the value that corresponds to the saturated electrolyte.

Changes in impedance are slower when the film involves a high-viscosity (HV) fluid (Fig. 4) as the contact line recedes at a lower rate in fluids of higher viscosity (see also Basu et al. 1996). The electrical impedance data gathered with the paraffin oil film



**Fig. 3.** Crude oil films after rupture



**Fig. 4.** Evolution in the electrical impedance of a water droplet as result of film breaking and ion hydration

do not seem to reach the asymptotic impedance of brine, probably due to changes in drop geometry or electrode contamination.

The diffusion of hydrated ions in water is a very slow process and it cannot explain the short reaction times observed in electrical measurements (Fig. 4). A possible explanation is the focusing of electrical current paths along the more conductive hydrated salt surface. This is explored using a two-dimensional finite element solution of Laplace's equation before and after the rupture of the film (Fig. 5). Before film rupture, the fluid in the droplet is modeled with a homogeneous conductivity  $1 \times 10^{-3}$  S/m [Fig. 5(b)]. After film rupture, the droplet is modeled with two layers: the bottom 0.5 mm thick layer is an electrolyte with conductivity  $1 \times 10^{-2}$  S/m, and the rest of the drop has the same initial conductivity  $1 \times 10^{-3}$  S/m. These finite element results confirm that film breakage and ion hydration cause high current density near the salt surface (arrows in the figure). These results support the use of an equivalent circuit analysis to model the impedance time response. In this lumped model, elemental resistances  $R$  are related to lengths, i.e., the film rupture length and the water path length, and a low-resistance element is used to represent the salt-water interface. The model fails to predict the observed time response. Therefore, the almost instantaneous effect of hydration on the measured impedance highlights the strongly dynamic nature of film rupture and the generation of advective currents within the water droplet.

### Optical Microscopy

Table 4 lists film thicknesses determined for different substrates and fluids (based on gravimetric techniques). Fig. 6 summarizes the average time determined for the rupture of oil films on different minerals. Fig. 7 shows the effect of surfactants. The following observations can be made:

1. The attained film thickness is controlled by the viscosity of the fluid (Table 4). Mineralogy plays a secondary role; calcite tends to produce the thickest films and biotite the thinnest films.
2. The film rupture time is strongly dependent on the properties of the nonwetting fluid forming the film. In particular, the lower the viscosity, the faster the film breaks (Fig. 6).
3. The type of substrate has an important effect on the film rupture time, as well (Fig. 6). Except for quartz, the rupture time correlates with the mineral's affinity for water, as indicated by the contact angle. The mineral affinity for the organic fluid explains the stronger time for film rupture observed in quartz (Table 3). For salt crystals, the time for film rupture (optical and impedance measurements) is less than

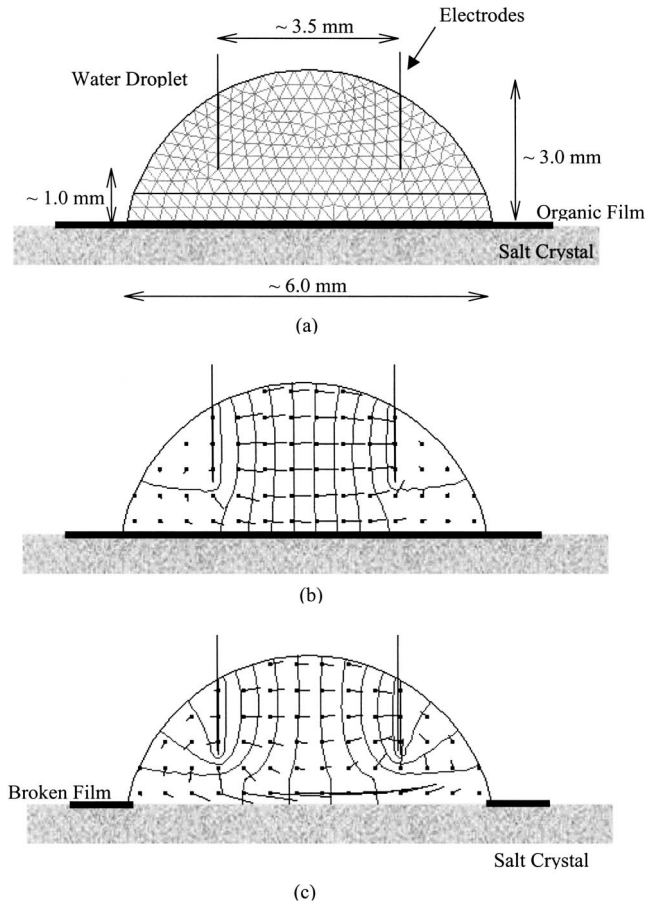


**Fig. 5.** Two-dimensional finite element model: Water droplet with two electrodes. (a) Geometry and mesh; (b) Equipotential lines and current density vectors before film rupture; and (c) Equipotential lines and current density vectors after film rupture (an electrolyte is assumed in the lower part of the water droplet).

5 s. There is a small difference between the rupture time for films on glass (amorphous silica) and quartz (silica tetrahedra).

4. The film tends to break faster when the wetting fluid is water-detergent than when it is deionized water or isopropyl alcohol (Fig. 7). Water and the water-detergent solution form drops on the films, but the isopropyl alcohol spreads over the films. The sequential order for film rupture is similar for all wetting fluids.

**Table 4.** Crude Oil Film Thickness on Different Solid Surfaces

Solid	Film thickness ( $\mu\text{m}$ )		
	LV oil $\eta=2.6 \text{ cm}^2/\text{s}$	MV oil $\eta=24 \text{ cm}^2/\text{s}$	HV oil $\eta=3,000 \text{ cm}^2/\text{s}$
Salt	$1.9 \pm 0.3$	$4.3 \pm 0.5$	$6.2 \pm 0.7$
Muscovite	$2.6 \pm 0.4$	$6.4 \pm 0.9$	$8.7 \pm 0.7$
Biotite	$1.6 \pm 0.5$	$2.5 \pm 0.9$	$5.0 \pm 2.0$
Calcite	$1.6 \pm 0.4$	$8.1 \pm 2.4$	$10.1 \pm 4.2$
Quartz	$1.4 \pm 0.5$	$4.4 \pm 2.0$	$5.7 \pm 1.0$
Glass	$1.6 \pm 0.1$	$4.3 \pm 0.3$	$4.7 \pm 0.8$
Plexiglas	$1.7 \pm 0.5$	$6.6 \pm 1.1$	$8.2 \pm 1.2$

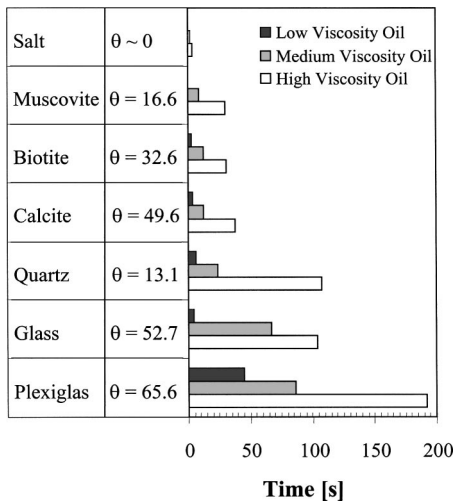


**Fig. 6.** Time for film rupture after water is added for different minerals. The tabulated contact angles correspond to mineral-water interface in air (Table 3).

### Discussion: Contact Angle and Film Instability

The contact angle  $\theta$ , the variation of the disjoining pressure  $\Pi$  with distance away from the surface  $h$ , and the interfacial tension  $\sigma_{OW}$  are related as predicted by the Young-Dupre equation (see Basu and Sharma 1996; Adamson and Gast 1997; Bergeron 1999)

$$\cos \theta = 1 - \frac{1}{\sigma_{OW}} \int_{h_0}^{\infty} \Pi dh \quad (6)$$

where  $h_0$  is the minimum stable film thickness (it is the result of all participating intermolecular forces). Note that the Young-Dupre equation relates the changes in the disjoining pressure (prior to film instability) to the contact angle (after film rupture).

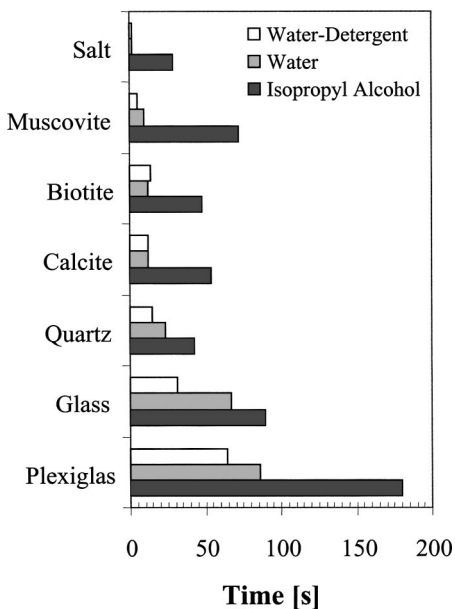


**Fig. 7.** Time for film rupture in the case of crude oil of medium viscosity (MV) ( $\eta=24 \text{ cm}^2/\text{s}$ ) for different minerals. The invading fluids are water, a water-detergent solution, and isopropyl alcohol.

The stability of a thin film coating a solid surface in the presence of a wetting fluid is determined by the complex interaction between the participating forces, as captured in the disjoining/conjoining pressure  $\Pi$ . Since forces are distance dependent, film instability depends on film thickness (Table 4; see Reiter et al. 1999); therefore, suboptical surface roughness can affect the observed response. In addition, the data show that mineral characteristics affect the time for film rupture as well. First, calcite and biotite exhibit similar rupture times, even though the film thicknesses on these substrates are the most different (Table 4). Second, the time for film rupture tends to decrease for the more hydrophilic substrates (Fig. 6).

Experimental results in Fig. 6 show that the higher the viscosity of the organic fluid, the higher the difficulty in displacing it from the mineral surface. Basu et al. (1996) and Lunn and Kueper (1999) made similar observations in macroscopic studies of oil displacement in porous media.

The presence of a surfactant such as detergent modifies the interfacial tension and favors the wetting of surfaces (Fig. 7), resulting in lower film rupture times. Surfactants accumulate at the interface with their hydrophilic head in contact with the aqueous solution and their hydrophobic tails oriented away from the film. Together with the surfactant, ions present in commercial detergents adsorb at the interface and modify the electrostatic forces. Then the force balance and the time for film rupture change. When holes appear in the film the surfactant moves onto the mineral surface and reduces the adhesion between mineral and oil.

The attraction forces between the mineral and surrounding media try to reduce the intermediate film thickness, while repulsive forces try to increase it (gravity and differences in fluid mass density also affect film thickness). In this study, the organic film prevents the formation of double layers on the mineral surface, there is no osmotic pressure and van der Waals forces prevail; thus, the free energy  $G$  per unit area is

$$G = - \frac{A_{12(3)}}{12\pi h^2} \quad (7)$$

where  $A_{12(3)}$  is the Hamaker constant between media "1" and "2," across the medium "3" (i.e., the film), and  $h$  is the film thickness. The Hamaker constant  $A_{12(3)}$  may be obtained from the Hamaker constant of each phase interacting across air (Lyklema 1991)

$$A_{12(3)} = (\sqrt{A_{11}} - \sqrt{A_{33}})(\sqrt{A_{22}} - \sqrt{A_{33}}) \quad (8)$$

If media "1" and "2" are the same, the Hamaker constant  $A_{ii}$  is always positive; thus, there is attraction between two layers of the same nature. The Hamaker constant for three different phases  $A_{12(3)}$  is negative when  $A_{11} > A_{33} > A_{22}$  or  $A_{11} < A_{33} < A_{22}$ . The permittivity of the three media determines the magnitude and sign of the Hamaker constant (note that the resultant van der Waals force may not be attraction). This explains differences in time for film rupture for a given organic and substrate, when reached by different fluids.

The adhesion energy per unit area between two identical surfaces separated by a liquid is equal to the work required to form two liquid-air interfaces  $= 2\sigma_{lv}$ . An expression for the Hamaker constant  $A_{ii(3)}$  in terms of the interfacial tension  $\sigma_{lv}$  can be derived by comparing this work to the free energy  $G$  when van der Waals forces dominate [Eq. (7); details in Israelachvili 1992]

$$A_{ii(3)} \approx 24\pi\sigma_{lv}D_0^2 \quad (9)$$

**Table 5.** Hamaker Constant  $A_{12(3)}$  at Temperature  $T=20^\circ\text{C}$ 

Mineral	$\kappa'^a$	Hamaker constant $A_{12(3)}(10^{-20} \text{ J})$		
		M-W (O)	M-WD (O)	M-IA (O)
Calcite	7.50–8.70	0.16–0.17	0.16–0.17	0.15–0.16
Quartz	4.49–5.06	0.10–0.11	0.10–0.11	0.09–0.11
Biotite	10.30	0.19	0.19	0.17
Muscovite	6.20–8.00	0.14–0.16	0.14–0.16	0.13–0.15

Note: M=mineral, O=crude oil ( $\kappa'=2.2$ ), W=deionized water ( $\kappa'=78.5$ ), WD=water-detergent solution ( $\kappa'\approx 78.5$ ), IA=isopropyl alcohol ( $\kappa'=34.7$ ).

<sup>a</sup>From Parkhomenko 1967.

where  $D_0$  approaches the interatomic distance (for nonpolar fluids,  $D_0\approx 0.16 \text{ nm}$ ). Therefore, the Hamaker constant for a given liquid-mineral interface is related to the liquid-vapor interfacial tension for the liquid.

If the van der Waals force prevails, unstable thin film conditions,  $\partial^2 G/\partial h^2 < 0$ , require that  $A_{12(3)} > 0$ . In physical terms, when the computed Hamaker constant is positive,  $A_{12(3)} > 0$ , the flooding fluid is attracted to the mineral surface, displaces the organic fluid, and causes the rupture of the thin film. Table 5 lists the computed Hamaker constant  $A_{12(3)}$  for calcite, quartz, muscovite, and biotite with water, water-detergent, and isopropyl alcohol across the oil film. The values for the Hamaker constant  $A_{ii}$  used in Eq. (8) are calculated on the basis of the Lifshitz theory (see Israelachvili 1992). Observe that in all cases  $A_{12(3)}$  is positive; therefore, thin film rupture is predicted.

The faster the rate at which the film thins,  $\partial h/\partial t$ , the shorter the time for film rupture. Film thinning depends on the disjoining pressure, the viscosity of the organic fluid in the thin film  $\eta$ , the thickness of the film  $h$  (m), and the length scale for the flooded region  $L$  (m). When van der Waals attraction prevails, dimensional considerations predict

$$\frac{\partial h}{\partial t} \propto \frac{A_{12(3)}}{\eta h L} \quad (10)$$

The following observations can be made. First, film rupture is faster in thinner films made of lower-viscosity fluids (Fig. 6). Second, film rupture localizes because the smaller the imprint of the flooded region,  $L$ , the higher the rate of thinning, leading to the formation of holes (Fig. 3; in addition, the thinner the film, the higher the attraction force). And third, the rate of film rupture depends on interfacial tensions [hinted by the relation between the Hamaker constant and interfacial tension in Eq. (9), and confirmed with experimental data in Fig. 7].

## Conclusions

Various surface processes and concepts in mixed fluid conditions are intimately related. These include interfacial tension, wettability, contact angle, capillary pressure, disjoining pressure, and thin film instability. Results obtained in this study indicate the following.

- The liquid-vapor interfacial tension plays a critical role in defining contact angle and wettability. Some minerals such as quartz and muscovite show a higher propensity to be wetted by fluids of any kind than other minerals such as calcite.
- The disjoining pressure encompasses all intermolecular forces and determines the stability of thin films. There is a critical

thickness for film stability. Instability develops when  $\partial \Pi/\partial h > 0$ ,  $\partial^2 G/\partial h^2 < 0$ , or  $A_{12(3)} > 0$  (if van der Waals forces prevail).

- Film rupture starts with the development of holes, followed by a sudden instability, and the transformation of the fluid from a thin film into droplets. The rate for film thinning leading to rupture depends on the mineral and the fluids (i.e.,  $A_{12(3)}$ ), and on the viscosity of the organic fluid that makes the thin film (higher-viscosity fluids are more difficult to displace from mineral surfaces). The thinning rate accelerates as the thickness gets smaller and with the smaller imprint of the flooding fluid.
- There is a time scale associated with film rupture. The presence of detergent in the displacing fluid decreases the rupture time of organic films over mineral surfaces.
- The indirect determination of film rupture can be conducted with electric impedance measurements. In this study the methodology was implemented at the microscale within a droplet. This measurement highlights the development of advective currents within the water drop during film rupture.

## Acknowledgments

Support for this research was provided by the Agencia Córdoba Ciencia, CONICET (Argentina), and the National Science Foundation (USA).

## References

- Abdul, A., Gibson, T., and Rai, D. (1990). "Selection of surfactants for the removal of petroleum products from shallow sandy aquifers." *Ground Water*, 28(6), 920–926.
- Abriola, L. M., Dekker, T., and Pennell, K. D. (1993). "Surfactant-enhanced solubilization of residual dodecane in soil columns. 2. Mathematical modeling." *Environ. Sci. Technol.*, 27(12), 2341–2351.
- Adamson, A. W., and Gast, A. P. (1997). *Physical chemistry of surfaces*, 6th Ed., Wiley, New York.
- Anderson, W. G. (1986). "Wettability literature survey—Part 2: Wettability measurement." *JPT*, 38(12), 1246–1262.
- Arman, A. (1992). "A review of remediation technologies in the USA." *Environmental Geotechnology*, Balkema, Rotterdam, The Netherlands, 385–389.
- Basu, S., Nandakumar, K., and Masliyah, J. H. (1996). "A study of oil displacement on model surfaces." *J. Colloid Interface Sci.*, 182(439), 82–94.
- Basu, S., and Sharma, M. M. (1996). "Measurement of critical disjoining pressure for dewetting of solid surfaces." *J. Colloid Interface Sci.*, 181(401), 443–455.
- Bergeron, V. (1999). "Forces and structure in thin liquid soap films." *J. Phys.: Condens. Matter*, PII:S0953-8984(99), R215–R238.
- Cho, G. C., and Santamarina, J. C. (2001). "Unsaturated particulate materials—Particle level studies." *J. Geotech. Geoenviron. Eng.*, 127(1), 84–96.
- Corey, A. T. (1986). "Mechanics of immiscible fluids in porous media." *Rep., Water Resources Publications*, Highlands Ranch, Colo.
- CRC Handbook. (1988). *Handbook of chemistry and physics*, R. C. Weast, ed., CRC Press, Boca Raton, Fla.
- Defay, R., and Prigogine, I. (1966). *Surface tension and adsorption*, Wiley, New York.
- Drelich, J., Miller, J. D., and Good, R. J. (1996). "The effect of drop (bubble) size on advancing and receding contact angles for heterogeneous and rough solid surfaces as observed with sessile-drop and captive-bubble techniques." *J. Colloid Interface Sci.*, 179(186), 37–50.
- Dullien, F. A. L. (1992). *Porous media fluid transport and pore structure*, 2nd Ed., Academic, New York.

- Ethington, E. F. (1990). "Interfacial contact angle measurements of water, mercury, and 20 organic liquids on quartz, calcite, biotite, and Ca-montmorillonite substrates." *Rep., USGS*, 90-409, 1-18.
- Extrand, C. W. (1998). "A thermodynamic model for contact angle hysteresis." *J. Colloid Interface Sci.*, 207(CS985743), 11-19.
- Extrand, C. W., and Kumagai, Y. (1997). "An experimental study of contact angle hysteresis." *J. Colloid Interface Sci.*, 191(CS974935), 378-383.
- Ghatak, A., Khanna, R., and Sharma, A. (1999). "Dynamics and morphology of holes in dewetting of thin films." *J. Colloid Interface Sci.*, 212, 483-494.
- Irwin, R., VanMouwerik, M., Stevens, L., Seese, M., and Basham, W. (1997). "Environmental contaminants encyclopedia." *Rep., National Park Service, Water Resources Division*, Fort Collins, Colo.
- Israelachvili, J. (1992). *Intermolecular and surface forces*, 2nd Ed., Academic, New York.
- Klein, C., and Hurlbut, C. S. (1999). *Manual of mineralogy (after James D. Dana)*, 21st Ed., Wiley, New York.
- Kwok, D. Y., and Neumann, A. W. (1999). "Contact angle measurement and contact angle interpretation." *Adv. Colloid Interface Sci.*, 81, 167-249.
- Lunn, S., and Kueper, B. (1999). "Manipulation of density and viscosity for the optimization of DNAPL recovery by alcohol flooding." *J. Contam. Hydrol.*, 38(4), 427-445.
- Lyklema, J. (1991). *Fundamentals of interface and colloid science, Vol. II: Solid-liquid interfaces*, Academic, New York.
- Mani, V., and Mohanty, K. K. (1997). "Effect of the spreading coefficient on three-phase flow in porous media." *J. Colloid Interface Sci.*, 187(CS964700), 46-56.
- Martel, R., Gélinaas, P. J., and Desnoyers, J. E. (1998). "Aquifer washing by micellar solutions: 1 Optimization of alcohol-surfactant-solvent solution." *J. Contam. Hydrol.*, 29(4), 319-346.
- Mercer, J. W., and Cohen, R. M. (1990). "A review of immiscible fluids in the subsurface: Properties, models, characterization and remediation." *J. Contam. Hydrol.*, 6, 107-163.
- Morrow, N. R. (1990). "Wettability and its effect on oil recovery." *JPT*, 42(12), 1476-1484.
- Parkhomenko, E. I. (1967). *Electrical properties of rocks*, Plenum, New York.
- Pennell, K. D., Abriola, L. M., and Weber, W. (1993). "Surfactant-enhanced solubilization of residual dodecane in soil columns. 1. Experimental investigation." *Environ. Sci. Technol.*, 27(12), 2332-2340.
- Pennell, K. D., Pope, G. A., and Abriola, L. M. (1996). "Influence of viscous and buoyancy forces on the mobilization of residual tetrachloroethylene during surfactant flushing." *Environ. Sci. Technol.*, 30(4), 1328-1335.
- Reiter, G., Sharma, A., Casoli, A., David, M., Khanna, R., and Auroy, P. (1999). "Thin film instability induced by long-range forces." *Langmuir*, 15(7), 2552-2558.
- Robin, M., Rosenberg, E., and Fassi-Fihri, O. (1995). "Wettability studies at pore level: A new approach by use of cryo-SEM." *SPE Formation Evaluation Rep.*, 10, 11-19.
- Sharma, A., and Reiter, G. (1996). "Instability of thin polymer films on coated substrates: Rupture, dewetting, and drop formation." *J. Colloid Interface Sci.*, 178(133), 383-399.
- Shaw, D. (1977). *Introduction to colloid and surface chemistry*, 2nd Ed., Butterworth, London.
- Tsekov, R., and Schulze, H. (1997). "Hydrophobic forces in thin liquid films: Adsorption contribution." *Langmuir*, 13(21), 5674-5677.
- Udell, K. S., Grubb, D. G., and Sitar, N. (1995). "Technologies for in situ cleanup of contaminated sites." *Cent. Eur. J. Public Health*, 2, 67-76.
- Zettlemoyer, A. (1969). *Hydrophobic surfaces*, Kendall Award Symposium on Hydrophobic Surfaces, 155th Meeting of the American Chemical Society, San Francisco, Academic, New York.